Electronic Supplementary Material (ESI) for Chemical Communications.

Electronic supplementary information for: Negative Linear Compressibility Exhibited by the Hybrid Perovskite $[(NH_2)_3C]Er(HCO_2)_2(C_2O_4)$]

Thomas J. Hitchings,[a] Rebecca Scatena,[b] David R. Allan,[b] Andrew B. Cairns [c,d] and Paul J. Saines[a]*

[a] School of Chemistry and Forensic Science, University of Kent, Canterbury, Kent, CT2 7NH, UK.

[b] Diamond Light Source Ltd., Harwell Science and Innovation Campus, Didcot, Oxfordshire, UK.

[c] Department of Materials, Imperial College London, South Kensington Campus,

London, SW7 2AZ, UK

[d]London Centre for Nanotechnology, Imperial College London, London SW7 2AZ, U.K.

Experimental

Synthesis

Single crystalline samples of [A]Er(HCO_2)$_2$(C_2O_4), where A = [(NH_2)$_3$C] and [(CH_3)$_2$$NH_2$], were produced by solvothermal synthesis methods.[1] For A = [(CH_3)$_2$$NH_2$], **DMA**, erbium nitrate pentahydrate (0.8867 g, 2 mmols), oxalic acid (0.1800 g, 2 mmols) and sodium carbonate (0.0846 g, 2 mmols) were added with a 1:1 ratio water:DMF (6 mL) , to a 23 mL stainless steel autoclave lined with a Teflon sleeve. Where [A] = [(NH_2)$_3$C], **GUA**, the same procedure was followed at half concentrations with the addition of guanidinium carbonate (0.0902 g, 0.5 mmols). The reactions were both placed in an oven for 72 hours at 150 °C and 100 °C respectively. During this process the temperature and autogenous pressure facilitated the degradation of the DMF solvent into dimethylammonium and formate constituents.

Attempts were made to substitute the cation for other small amines, but the degradation of the DMF solvent, resulted in the **DMA** form in each case. By swapping out the DMF for water, samples of **GUA** and **DMA** were able to be produced, but single crystalline samples of [A]Er(HCO)$_2$(C_2O_4) where [A] ≠ **GUA** or **DMA**, were unable to be found by this method. Where [A] = urea, [NH_4]Er(C_2O_4)$_2$ ·(H_2O) was found to crystalise in the monoclinic *P*2/*n* as a 2D layered oxalate framework and is isostructural to the reported yttrium analogue.[2]

All reactions yielded pale pink crystals of varying sizes.

Variable pressure single crystal X-ray diffraction

The variable pressure diffraction experiment was carried out on the I19 beamline at the Diamond Light Source.[3] Good quality single crystals were loaded into diamond anvil cells (DAC) with two opposing diamonds with culet tips, between which a tungsten gasket with a 200 μm hole drilled into it was sandwiched to form the sample chamber. An amorphous ruby chip was also loaded into the DACs as a pressure calibrant, tracked by fluorescence spectroscopy, see Table S3 for values. Following an ambient pressure collection of each sample, pressure transmitting media, 4:1 methanol:ethanol was introduced to the sample chambers and sealed. Between collections, the screws of the DAC were tightened, and the pressure within the DAC was allowed to stabilise for a minimum of 20 minutes. Data reduction and space group determination was completed on the beamline I19 using Xia2[4] with peak integration performed using DIALS.[5,6] Structures were solved and refined using direct methods with SHELXS and refined using SHELXL in the Olex2 graphical user interface.[7,8] Several restraints are used including rigid bond restraints and isotropic restraints to restrain the ADPs of the atoms to be approximately isotropic due to the gaps in reciprocal space present from using a diamond anvil cell.

A final data point for **GUA** was collected at 3.34(16) GPa that indexed with a much smaller unit cell and contraction in *c*, with full structural solution challenging, signifying an upper pressure limit to the NLC behaviour, as well as the integrity of the crystal. The lattice parameters were indexed as *a* = 7.428(6) Å, *b* = 6.293(4) Å, *c* = 18.51(6) Å, *V* = 865(3) Å^3 and not included in any of the equation of state fits.

Similarly, a final phase III of **DMA** was found above 1.40(10) GPa with data points collected at 1.80(10) GPa and 2.18(10) GPa. These unit cells were indexed, *a* = 7.20(3) Å, *b* = 10.13(2) Å, *c* = 9.4(3) Å, *V* = 681(4) Å3 and a = 6.96(7) Å, b = 9.84(4) Å, c = 9.16(4) Å, V = 626(7) Å3, respectively, but full structural solution was not possible. Upon increasing pressure above 1.40(10) GPa, cell volume increases, which typically indicates that the pressure transmitting medium penetrates the crystal, a behaviour usually seen in porous systems.[9] These data points were also excluded from fittings to the equations of state.

Table S1: Crystallographic tables for **GUA**

Pressure	**Ambient**	**0.08 GPa**	**0.16 GPa**	**0.33 GPa**	**0.55 GPa**
Identification code	11_GUA03	12_GUA03	22_GUA03	24_GUA03	30_GUA03
Empirical formula	$C_5H_8ErN_3O_8$	$C_5H_8ErN_3O_8$	$C_5H_8ErN_3O_8$	$C_5H_8ErN_3O_8$	$C_5H_8ErN_3O_8$
Formula weight	405.40	405.40	405.40	405.40	405.40
Temperature/K	300	300	300	300	300
Crystal system	orthorhombic	orthorhombic	orthorhombic	orthorhombic	orthorhombic
Space group	*Pcca*	*Pcca*	*Pcca*	*Pcca*	*Pcca*
a / Å	8.49580(10)	8.45510(13)	8.41540(18)	8.35830(18)	8.3154(2)
b / Å	6.59460(10)	6.58400(7)	6.57240(8)	6.55850(8)	6.54900(9)
c / Å	19.201(2)	19.2134(18)	19.210(2)	19.218(2)	19.234(3)
α / °	90	90	90	90	90
β / °	90	90	90	90	90
γ / °	90	90	90	90	90
Volume /Å^3	1075.78(11)	1069.58(10)	1062.49(14)	1053.47(13)	1047.43(15)
Z	4	4	4	4	4
ρ_{calc} g/cm^3	2.503	2.518	2.534	2.556	2.571
μ /mm^{-1}	2.835	2.851	2.871	2.895	2.912
F(000)	764.0	764.0	764.0	764.0	764.0
Crystal size/mm^3	0.103 × 0.036 × 0.011	0.103 × 0.036 × 0.011	0.103 × 0.036 × 0.011	0.103 × 0.036 × 0.011	0.103 × 0.036 × 0.011
Radiation	λ = 0.4859	λ = 0.4859	λ = 0.4859	λ = 0.4859	λ = 0.4859
2Θ range for data collection / °	4.222 to 52.968	4.23 to 53.064	4.236 to 52.13	4.246 to 51.292	4.252 to 53.38
Index ranges	-12 ≤ h ≤ 14, -12 ≤ k ≤ 10, -13 ≤ l ≤ 13	-12 ≤ h ≤ 14, -10 ≤ k ≤ 12, -13 ≤ l ≤ 13	-14 ≤ h ≤ 12, -10 ≤ k ≤ 11, -13 ≤ l ≤ 13	-11 ≤ h ≤ 13, -11 ≤ k ≤ 10, -13 ≤ l ≤ 13	-14 ≤ h ≤ 12, -10 ≤ k ≤ 12, -13 ≤ l ≤ 13
Reflections collected	5278	5151	5174	5142	5077
Independent reflections	1019 [R_{int} = 0.0311, R_{sigma} = 0.0235]	986 [R_{int} = 0.0312, R_{sigma} = 0.0245]	976 [R_{int} = 0.0325, R_{sigma} = 0.0296]	971 [R_{int} = 0.0307, R_{sigma} = 0.0273]	988 [R_{int} = 0.0288, R_{sigma} = 0.0223]
Data/restraints/parameters	1019/31/79	986/31/79	976/31/79	971/31/79	988/31/79
Goodness-of-fit on F^2	1.125	1.076	1.032	1.032	1.031
Final R indexes [I>=2σ (I)]	R_1 = 0.0197, wR_2 = 0.0498	R_1 = 0.0180, wR_2 = 0.0514	R_1 = 0.0197, wR_2 = 0.0540	R_1 = 0.0207, wR_2 = 0.0578	R_1 = 0.0273, wR_2 = 0.0876
Final R indexes [all data]	R_1 = 0.0348, wR_2 = 0.0591	R_1 = 0.0274, wR_2 = 0.0528	R_1 = 0.0341, wR_2 = 0.0562	R_1 = 0.0370, wR_2 = 0.0623	R_1 = 0.0411, wR_2 = 0.0948
Largest diff. peak/hole / e Å^{-3}	0.67/-0.68	0.57/-0.39	0.65/-0.56	0.44/-0.53	0.58/-0.61

Table S1 continued:

Pressure	**0.78 GPa**	**1.03 GPa**	**2.01 GPa**	**2.38 GPa**	**2.63 GPa**
Identification code	06_GUA04	07_GUA04	32_GUA03	34_GUA03	36_GUA03
Empirical formula	$C_5H_8ErN_3O_8$	$C_5H_8ErN_3O_8$	$C_5H_8ErN_3O_8$	$C_5H_8ErN_3O_8$	$C_5H_8ErN_3O_8$
Formula weight	405.40	405.40	405.40	405.40	405.40
Temperature/K	300	300	300	300	300
Crystal system	orthorhombic	orthorhombic	orthorhombic	orthorhombic	orthorhombic
Space group	*Pcca*	*Pcca*	*Pcca*	*Pcca*	*Pcca*
a / Å	8.2526(2)	8.1956(2)	7.8462(14)	7.801(2)	7.736(8)
b / Å	6.54270(17)	6.53400(18)	6.5142(11)	6.5107(13)	6.479(5)
c / Å	19.313(5)	19.322(5)	19.58(2)	19.64(2)	19.71(12)
α / °	90	90	90	90	90
β / °	90	90	90	90	90
γ / °	90	90	90	90	90
Volume /Å^3	1042.8(3)	1034.7(3)	1000.6(12)	997.5(11)	988(6)
Z	4	4	4	4	4
ρ_{calc} g/cm^3	2.582	2.602	2.691	2.700	2.726
μ / mm^{-1}	2.925	2.948	3.048	3.058	3.087
F(000)	764.0	764.0	764.0	764.0	764.0
Crystal size/mm^3	0.143 × 0.067 × 0.039	0.143 × 0.067 × 0.039	0.103 × 0.036 × 0.011	0.103 × 0.036 × 0.011	0.103 × 0.036 × 0.011
Radiation	λ = 0.4859	λ = 0.4859	λ = 0.4859	λ = 0.4859	λ = 0.4859
2Θ range for data collection/°	4.256 to 50.922	4.262 to 51.944	4.274 to 33.944	4.278 to 25.204	4.298 to 31.202
Index ranges	-13 ≤ h ≤ 14, -10 ≤ k ≤ 9, -8 ≤ l ≤ 8	-14 ≤ h ≤ 13, -11 ≤ k ≤ 9, -8 ≤ l ≤ 8	-9 ≤ h ≤ 9, -7 ≤ k ≤ 7, -12 ≤ l ≤ 12	-7 ≤ h ≤ 7, -5 ≤ k ≤ 5, -10 ≤ l ≤ 10	-8 ≤ h ≤ 8, -7 ≤ k ≤ 7, -11 ≤ l ≤ 11
Reflections collected	5059	4932	2932	1288	2407
Independent reflections	734 [R_{int} = 0.0334, R_{sigma} = 0.0219]	737 [R_{int} = 0.0330, R_{sigma} = 0.0238]	472 [R_{int} = 0.0585, R_{sigma} = 0.0698]	203 [R_{int} = 0.0981, R_{sigma} = 0.0796]	393 [R_{int} = 0.0761, R_{sigma} = 0.0475]
Data/restraints/parameters	734/45/67	737/45/67	472/65/79	203/93/63	393/88/63
Goodness-of-fit on F^2	1.093	1.103	0.827	0.772	1.113
Final R indexes [I>=2σ (I)]	R_1 = 0.0223, wR_2 = 0.0662	R_1 = 0.0279, wR_2 = 0.0811	R_1 = 0.0424, wR_2 = 0.1007	R_1 = 0.0420, wR_2 = 0.0992	R_1 = 0.1159, wR_2 = 0.2877
Final R indexes [all data]	R_1 = 0.0340, wR_2 = 0.0693	R_1 = 0.0438, wR_2 = 0.0865	R_1 = 0.0714, wR_2 = 0.1058	R_1 = 0.0635, wR_2 = 0.1038	R_1 = 0.1447, wR_2 = 0.3100
Largest diff. peak/hole / e Å^{-3}	0.32/-0.54	0.39/-0.99	0.66/-0.75	0.73/-0.44	1.46/-1.20

Table S2: Crystallographic tables for **DMA**

Pressure	**Ambient**	**0.08 GPa**	**0.16 GPa**	**0.22 GPa**	**0.37 GPa**
Identification code	03_DMA01	08_DMA01	12_DMA01	14_DMA01	16_DMA01
Empirical formula	$C_6H_{10}ErNO_8$	$C_6H_{10}ErNO_8$	$C_6H_{10}ErNO_8$	$C_6H_{10}ErNO_8$	$C_6H_{10}ErNO_8$
Formula weight	391.41	391.41	391.41	391.41	391.41
Temperature/K	300	300.00	300.00	300.00	300.00
Crystal system	monoclinic	monoclinic	monoclinic	monoclinic	monoclinic
Space group	*P*2/*n*	*P*2/*n*	*P*2/*n*	*P*2/*n*	*P*2/*n*
a / Å	9.1533(2)	9.1539(3)	9.1263(6)	9.1326(5)	9.1183(8)
b / Å	8.9945(16)	8.9987(19)	8.963(4)	8.974(4)	8.948(5)
c / Å	13.1812(2)	13.1797(2)	13.1305(7)	13.1405(6)	13.1042(7)
α / °	90	90	90	90	90
β / °	96.7470(10)	96.604(2)	96.440(4)	96.410(4)	96.446(5)
γ / °	90	90	90	90	90
Volume / $Å^3$	1077.68(19)	1078.5(2)	1067.3(5)	1070.2(5)	1062.5(6)
Z	4	4	4	4	4
$\rho_{calc}g/cm^3$	2.412	2.411	2.436	2.429	2.447
μ/mm^{-1}	2.826	2.824	2.853	2.846	2.867
F(000)	740.0	740.0	740.0	740.0	740.0
Crystal size/mm^3	0.253 × 0.142 × 0.134	0.253 × 0.142 × 0.134	0.253 × 0.142 × 0.134	0.253 × 0.142 × 0.134	0.253 × 0.142 × 0.134
Radiation	λ = 0.4859	λ = 0.4859	λ = 0.4859	λ = 0.4859	λ = 0.4859
2Θ range for data collection / °	3.518 to 51.192	3.522 to 51.252	3.538 to 42.452	3.536 to 42.502	3.542 to 40.622
Index ranges	-12 ≤ h ≤ 10, -4 ≤ k ≤ 4, -20 ≤ l ≤ 20	-12 ≤ h ≤ 10, -4 ≤ k ≤ 4, -20 ≤ l ≤ 20	-11 ≤ h ≤ 10, -4 ≤ k ≤ 4, -19 ≤ l ≤ 19	-11 ≤ h ≤ 10, -4 ≤ k ≤ 4, -19 ≤ l ≤ 19	-11 ≤ h ≤ 10, -4 ≤ k ≤ 4, -18 ≤ l ≤ 18
Reflections collected	5265	5341	4991	5013	4752
Independent reflections	1140 [R_{int} = 0.0232, R_{sigma} = 0.0166]	1180 [R_{int} = 0.0246, R_{sigma} = 0.0211]	1016 [R_{int} = 0.0338, R_{sigma} = 0.0285]	1027 [R_{int} = 0.0305, R_{sigma} = 0.0273]	959 [R_{int} = 0.0288, R_{sigma} = 0.0273]
Data/restraints/parameters	1140/93/148	1180/93/148	1016/135/148	1027/135/148	959/135/148
Goodness-of-fit on F^2	1.169	1.071	1.037	0.996	0.881
Final R indexes [I>=2σ (I)]	R_1 = 0.0205, wR_2 = 0.0667	R_1 = 0.0414, wR_2 = 0.1420	R_1 = 0.0409, wR_2 = 0.1414	R_1 = 0.0450, wR_2 = 0.1512	R_1 = 0.0519, wR_2 = 0.1540
Final R indexes [all data]	R_1 = 0.0245, wR_2 = 0.0679	R_1 = 0.0489, wR_2 = 0.1461	R_1 = 0.0534, wR_2 = 0.1458	R_1 = 0.0586, wR_2 = 0.1564	R_1 = 0.0664, wR_2 = 0.1664
Largest diff. peak/hole / e $Å^{-3}$	0.52/-0.36	1.33/-0.68	0.63/-0.47	0.86/-0.64	1.01/-0.99

Table S2 continued:

Pressure	**0.76 GPa**	**1.02 GPa**	**1.15 GPa**	**1.40 GPa**
Identification code	18_DMA01	20_DMA01	22_DMA01	24_DMA01
Empirical formula	$C_6H_{10}ErNO_8$	$C_6H_{10}ErNO_8$	$C_6H_{10}ErNO_8$	$C_6H_{10}ErNO_8$
Formula weight	391.41	391.41	391.41	391.41
Temperature/K	300	300.00	300.00	300.00
Crystal system	monoclinic	monoclinic	monoclinic	monoclinic
Space group	*P*2/*a*	*P*2/*a*	*P*2/*a*	*P*2/*a*
a / Å	9.1025(11)	9.0907(8)	9.0759(5)	9.0471(15)
b / Å	8.913(8)	8.903(6)	8.863(6)	8.792(11)
c / Å	6.5273(6)	6.5091(5)	6.4822(8)	6.4339(9)
α / °	90	90	90	90
β / °	96.442(7)	96.380(6)	96.228(5)	96.131(10)
γ / °	90	90	90	90
Volume / $Å^3$	526.2(5)	523.6(4)	518.3(4)	508.9(7)
Z	2	2	2	2
ρ_{calc} g/cm^3	2.470	2.483	2.508	2.555
μ /mm^{-1}	2.894	2.908	2.938	2.993
F(000)	370.0	370.0	370.0	370.0
Crystal size/mm^3	0.253 × 0.142 × 0.134	0.253 × 0.142 × 0.134	0.253 × 0.142 × 0.134	0.253 × 0.142 × 0.134
Radiation	λ = 0.4859	λ = 0.4859	λ = 0.4859	λ = 0.4859
2Θ range for data collection / °	4.294 to 40.664	4.304 to 38.436	4.322 to 38.4	4.354 to 34.276
Index ranges	-10 ≤ h ≤ 11, -3 ≤ k ≤ 3, -9 ≤ l ≤ 9	-11 ≤ h ≤ 10, -3 ≤ k ≤ 3, -8 ≤ l ≤ 8	-10 ≤ h ≤ 11, -3 ≤ k ≤ 3, -8 ≤ l ≤ 8	-10 ≤ h ≤ 10, -3 ≤ k ≤ 3, -7 ≤ l ≤ 7
Reflections collected	2338	2082	2052	1551
Independent reflections	453 [R_{int} = 0.0279, R_{sigma} = 0.0218]	397 [R_{int} = 0.0235, R_{sigma} = 0.0173]	401 [R_{int} = 0.0214, R_{sigma} = 0.0159]	306 [R_{int} = 0.0259, R_{sigma} = 0.0195]
Data/restraints/parameters	453/42/80	397/65/68	401/65/68	306/74/80
Goodness-of-fit on F^2	1.176	1.178	1.135	1.092
Final R indexes [I>=2σ (I)]	R_1 = 0.0521, wR_2 = 0.1529	R_1 = 0.0515, wR_2 = 0.1544	R_1 = 0.0567, wR_2 = 0.1666	R_1 = 0.0461, wR_2 = 0.1389
Final R indexes [all data]	R_1 = 0.0588, wR_2 = 0.1636	R_1 = 0.0581, wR_2 = 0.1615	R_1 = 0.0625, wR_2 = 0.1765	R_1 = 0.0534, wR_2 = 0.1460
Largest diff. peak/hole / e $Å^{-3}$	0.59/-0.59	0.48/-0.46	0.36/-0.46	0.34/-0.33

The unit cell of phase II was indexed in *P*2/*c* but transformed to *P*2/*a* by the transformation matrix shown in Equation S1 for consistency of *a* and *c* between phases.

$$\begin{pmatrix} a' \\ b' \\ c' \end{pmatrix} = \begin{pmatrix} 0 & 0 & 1 \\ 0 & -1 & 0 \\ 1 & 0 & 0 \end{pmatrix} \begin{pmatrix} a \\ b \\ c \end{pmatrix} \quad \text{(S1)}$$

Equation S1: Transformation matrix to convert the auto indexed phase II from *P*2/*c* to *P*2/*a*, non-standard setting.

Table S3: Ruby fluorescence λ_{max} values measured before and after collection and calculated pressure intervals within the diamond anvil cell.

GUA			DMA		
Identification Code	λ_{max} / nm	Pressure / GPa	Identification Code	λ_{max} / nm	Pressure / GPa
11_GUA03	694.15	0.0001	03_DMA01	694.12	0.0001
12_GUA03	694.18	0.08(10)	08_DMA01	694.15	0.08(10)
22_GUA03	694.21	0.16(10)	12_DMA01	694.18	0.16(10)
24_GUA03	694.27	0.33(10)	14_DMA01	694.20	0.22(10)
30_GUA03	694.35	0.55(10)	16_DMA01	694.255	0.37(10)
32_GUA03	694.91	2.01(10)	18_DMA01	694.395	0.76(10)
34_GUA03	695.02	2.38(10)	20_DMA01	694.49	1.02(10)
36_GUA03	695.09	2.63(10)	22_DMA01	694.54	1.15(10)
39_GUA03	695.39	3.34(10)	24_DMA01	694.63	1.40(10)
06_GUA04	694.39	0.78(10)	26_DMA01	694.84	1.80(10)
07_GUA04	694.50	1.03(10)	32_DMA01	694.905	2.18(10)

Comparability of systems exhibiting NLC behaviour is achieved by calculation of the isothermal compressibility coefficient (K_l) along each of the principal axes of compression (X1-3) over a given pressure range (∂p).[10,11] K_l is the magnitude of the rate of change in the principal axis of compression and is given by:

$$\mathrm{K_l} = \frac{1}{\mathrm{l}}\left(\frac{\partial \mathrm{l}}{\partial \mathrm{p}}\right)_{\mathrm{T}} \qquad \text{(S2)}$$

For systems of orthorhombic symmetry and higher, the principal axes will coincide with the crystallographic axes but for non-orthogonal monoclinic and triclinic systems, principal and crystallographic axes are not bound to align so the variations in cell angles as well as lengths must be considered. [10,11] The eigenvalues of the strain tensor are equivalent to the principal axis of compression in all cases.

Values of the bulk modulus, B_0, were extracted from fits of the cell volume changes with pressure to Birch–Murnaghan equations of state. A third-order fit was used for **GUA**, with a second-order fit used for **DMA** phases I and II due to the limited number of data points. Fits were carried out using EoSFit,[12,13] with V_0 fixed to the measured value. A second-order fit of **GUA** gave a value for B_0 = 24.4(10) GPa.

Table S4: The principal axis of compression eigenvalues, *K*, and error sigma, with their vector directions in terms of crystallographic direction **GUA**

	K / TPa^{-1}	σ / TPa^{-1}	*a*	*b*	*c*
X1 (K_a)	35.1485	3.7039	1	0	0
X2(K_b)	5.0907	0.5042	0	1	0
X3(K_c)	-10.0914	0.738	0	0	1
V	29.7764	1.3454			

Table S5: The principal axis of compression eigenvalues, *K*, and error sigma, with their vector directions in terms of crystallographic direction for phases I and II of **DMA**.

	K / TPa^{-1}	σ / TPa^{-1}	*a*	*b*	*c*
I					
X1	18.9828	11.7169	-0.7655	0	0.6435
X2	13.2612	10.2619	0	1	0
X3	6.6172	24.6713	0.8585	0	0.5127
V	49.558	9.2421			
II					
X1	36.9049	-++	-0.2397	0	0.9708
X2	43.1531	-++	0	1	0
X3	16.0517	-++	0.8526	0	0.5226
V	56.9369	7.5513			

++ not enough data points to reliably calculate errors.

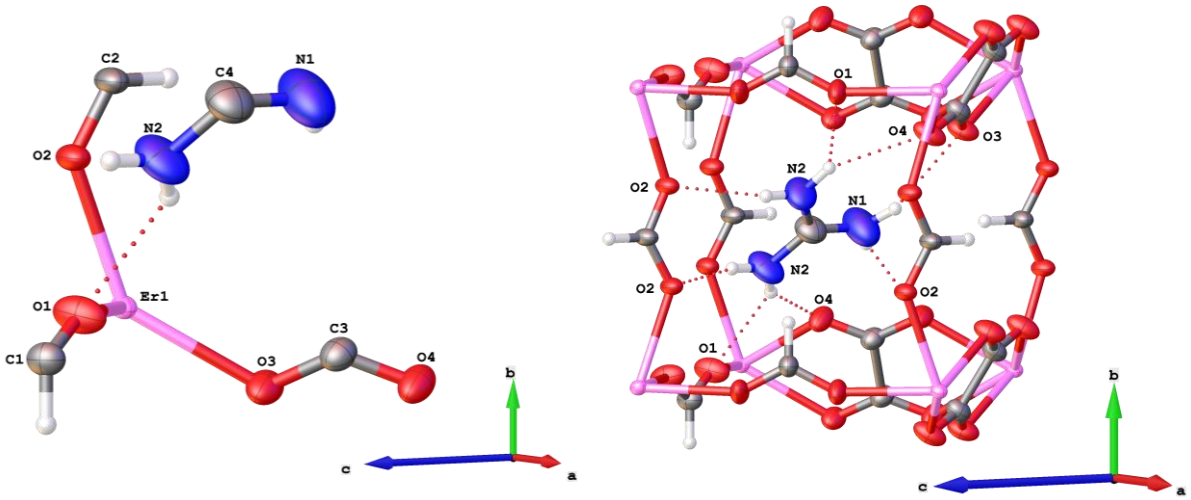

Figure S1: (left) asymmetric unit of **GUA** at ambient pressure (right) view to show the hybrid perovskite structure with atoms involved in host-guest interactions highlighted.

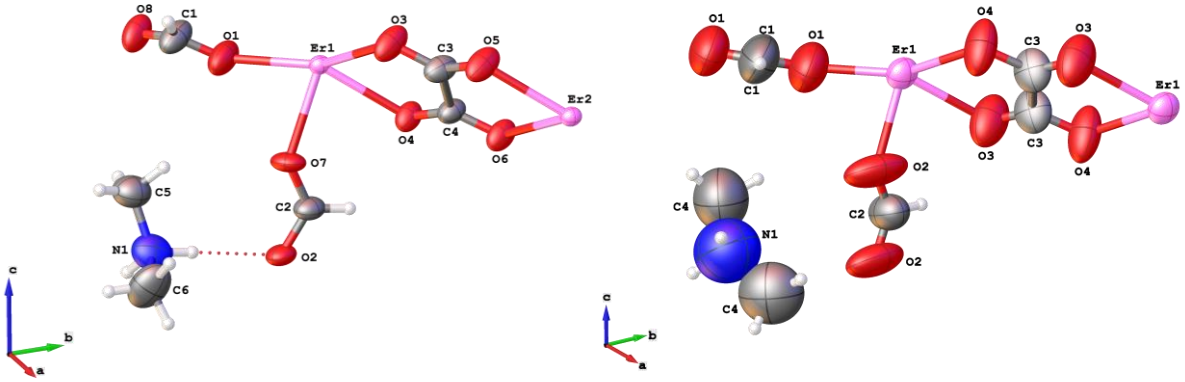

Figure S2: (left) asymmetric unit of **DMA** phase I with atom labels (right) the corresponding structure at phase II (0.76 GPa) showing which atoms become symmetrically equivalent and the rotation of the DMA cation.

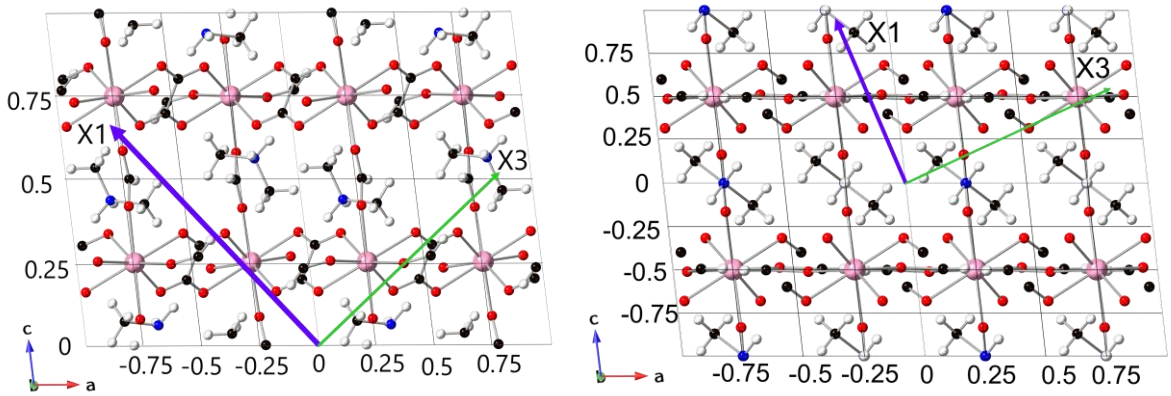

Fig. S3: (left) Phase I of **DMA** with the vectors outlined in Table S5, overlaid with the atomic structure model. (right) phase I of **DMA** with the vectors outlined in

Table S5 overlaid with the atomic structure model, showing a ~45° rotation around the *b*-axis of the principal compression axis with the phase transition.

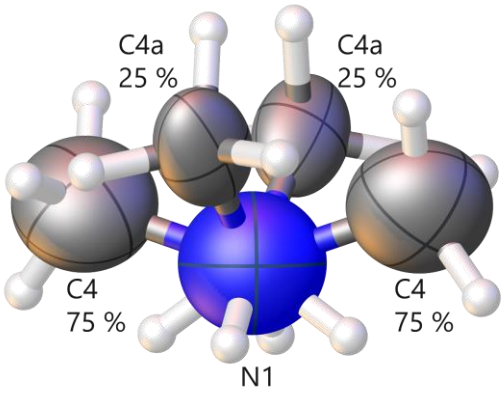

Figure S4: Disorder in the **DMA** A-site cation only modellable at 0.76 GPa. Disorder omitted from final model and is likely a consequence of remnant regions of phase I following the phase transition as the intensity of the single difference peak at this pressure decreases with increasing pressure.

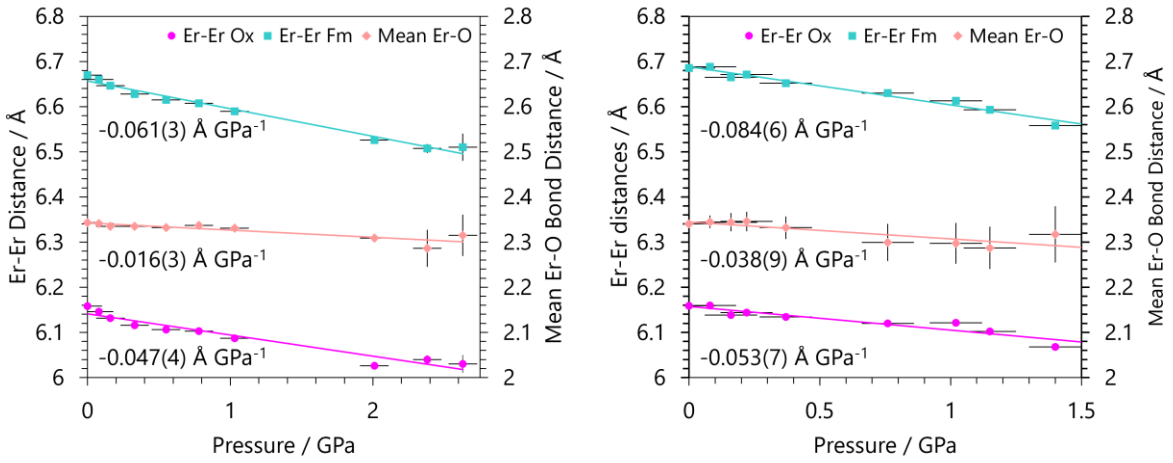

Figure S5: The changes in the Er-Er distances across the oxalate (Er-Er Ox) and formate (Er-Er Fm) linkers with increasing pressure and the shortest hydrogen bond host-guest interaction between the anionic framework for **a** (left) **GUA** and **b** (right) **DMA**, where in both cases errors on Er-Er distances are smaller than the marker size where not visible.

We note that the coordination polyhedra are relatively rigid, with the average rate of compression for the Er−O bond only ∼0.016(3) Å GPa^{-1} and ∼0.038(9) Å GPa^{-1}, for **GUA** and **DMA**, respectively, see Tables S6−S9.

Table S6: Changes in the dodecahedral Er environment with pressure for **GUA**.

Pressure / GPa	Er -O1 / Å	Er -O2 / Å	Er -O3 / Å	Er -O4 / Å	Mean Er -O Length / Å	Polyhedral Volume / Å³
0	2.273(7)	2.340(4)	2.363(6)	2.396(4)	2.343	22.692
0.08	2.272(6)	2.338(3)	2.366(3)	2.388(3)	2.341	22.634
0.16	2.258(6)	2.336(3)	2.365(5)	2.381(3)	2.335	22.482
0.33	2.262(7)	2.326(4)	2.372(5)	2.379(4)	2.335	22.467
0.55	2.265(9)	2.329(5)	2.361(5)	2.373(4)	2.332	22.377
0.78	2.284(10)	2.327(5)	2.366(6)	2.370(5)	2.337	22.492
1.03	2.263(15)	2.324(6)	2.366(9)	2.372(7)	2.331	22.311
2.01	2.27(3)	2.297(10)	2.31(2)	2.35(2)	2.31	21.66
2.38	2.14(6)	2.297(18)	2.32(5)	2.40(4)	2.29	20.88
2.63	2.29(8)	2.26(3)	2.33(4)	2.38(4)	2.32	21.95

Table S7: Changes in the dodecahedral Er environment with pressure for **DMA** Phase I, Er1.

Pressure / GPa	Er -O1 / Å	Er -O3 / Å	Er -O4 / Å	Er -O7 / Å	Mean Er -O Length / Å	Polyhedral Volume / Å³
0	2.295(10)	2.367(6)	2.362(7)	2.325(4)	2.337(5)	22.570
0.08	2.33(2)	2.347(12)	2.359(14)	2.339(9)	2.343(14)	22.78
0.16	2.36(4)	2.360(17)	2.37(2)	2.315(12)	2.35(2)	23.01
0.22	2.38(4)	2.334(17)	2.38(2)	2.311(13)	2.35(2)	23.04
0.37	2.34(4)	2.33(2)	2.35(3)	2.300(16)	2.33(3)	22.56

Table S8: Changes in the dodecahedral Er environment with pressure for **DMA** Phase I, Er2.

Pressure / GPa	Er -O2 / Å	Er -O5 / Å	Er -O6 / Å	Er -O8 / Å	Mean Er -O Length / Å	Polyhedral Volume / Å³
0	2.355(4)	2.349(8)	2.373(5)	2.298(9)	2.344(7)	22.802
0.08	2.355(9)	2.368(14)	2.348(11)	2.31(2)	2.346(14)	22.93
0.16	2.334(11)	2.36(2)	2.341(16)	2.31(3)	2.337(19)	22.61
0.22	2.335(12)	2.37(3)	2.320(16)	2.33(3)	2.34(2)	22.74
0.37	2.346(15)	2.36(3)	2.301(17)	2.32(4)	2.33(2)	22.53

Table S9: Changes in the dodecahedral Er environment with pressure for **DMA** Phase II.

Pressure / GPa	Er -O1 / Å	Er -O2 / Å	Er -O3 / Å	Er -O4 / Å	Mean Er -O Length / Å	Polyhedral Volume / Å³
0.76	2.16(7)	2.32(2)	2.41(4)	2.31(3)	2.30(4)	21.62
1.02	2.13(7)	2.33(3)	2.46(5)	2.27(3)	2.30(5)	21.62
1.15	2.15(8)	2.32(3)	2.45(5)	2.23(3)	2.29(5)	21.36
1.40	2.13(10)	2.39(3)	2.51(7)	2.24(5)	2.32(6)	22.31

Table S10: Hydrogen bond distances between the guanidinium cation and the anionic framework.

Pressure/ GPa	O3-N1/ Å	O2-N2/ Å	O1-N2/ Å	O4-N2 / Å
0	3.09(2)	3.014(13)	3.086(6)	3.130(11)
0.08	3.12(2)	3.043(9)	3.085(3)	3.120(7)
0.16	3.07(2)	3.025(10)	3.250(8)	3.113(8)
0.33	3.08(3)	3.027(11)	3.247(10)	3.122(9)
0.78	3.12(3)	3.003(16)	3.029(5)	3.099(12)
1.03	3.12(4)	3.01(2)	3.017(7)	3.12(4)
0.55	3.07(3)	3.023(13)	3.041(5)	3.104(10)
2.01	3.18(6)	3.00(4)	2.931(17)	3.21(4)
2.38	3.21(12)	3.00(8)	2.94(5)	3.21(8)
2.63	3.38(10)	3.07(8)	3.24(8)	3.16(8)

Table S11: Hydrogen bond distances between the dimethylammonium cation and the anionic framework.

Pressure/ GPa	O2-N1 / Å	O1-N1 / Å	O3-N1 / Å
0	3.023(14)	3.074(6)	2.992(12)
0.08	3.04(3)	3.115(13)	2.99(3)
0.16	3.04(5)	3.14(2)	3.05(4)
0.22	3.06(6)	3.14(3)	3.02(4)
0.37	2.94(6)	3.16(3)	3.12(5)
0.76			2.61(19)
1.02			2.70(19)
1.15			2.15(17)
1.40			2.01(10)

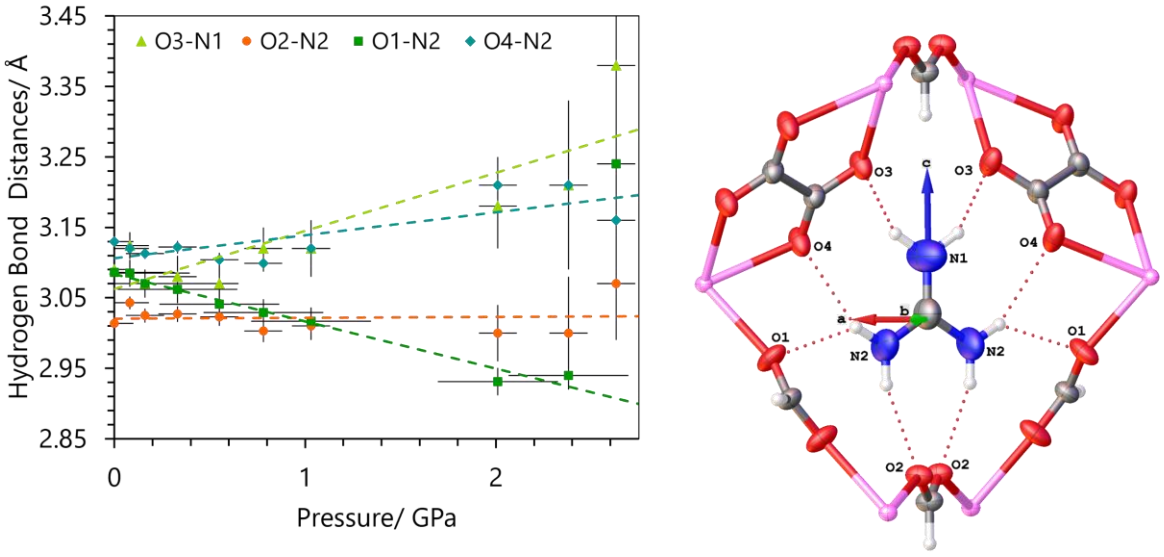

Figure S6: Hydrogen bonding in **GUA** with pressure, with relevant bonds labelled on the right, linear fits have been applied to guide the eye towards general trends.

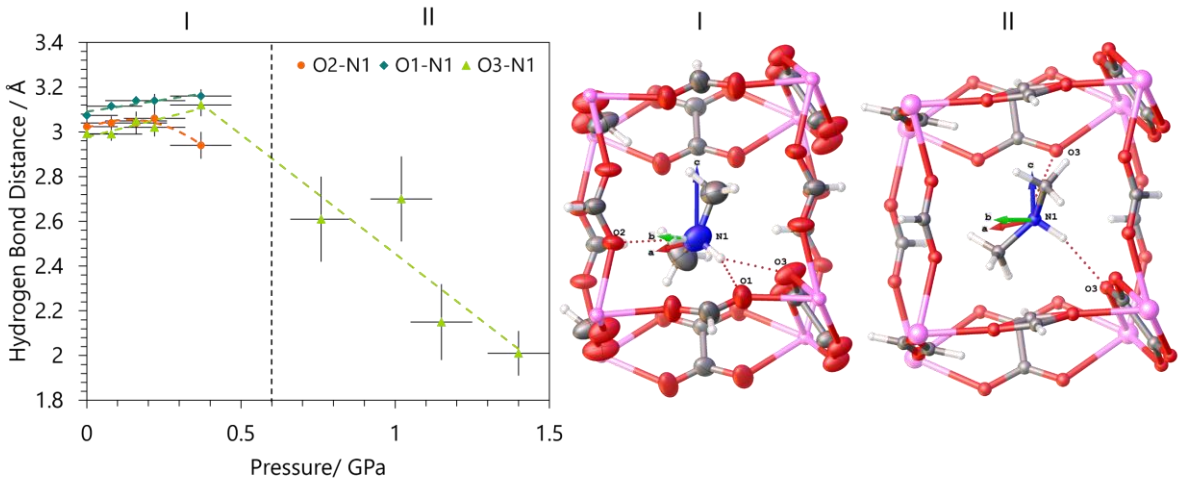

Figure S7: Hydrogen bonding between guest and framework for **DMA** phase I and II with increasing pressure, linear fits have been applied to guide the eye.

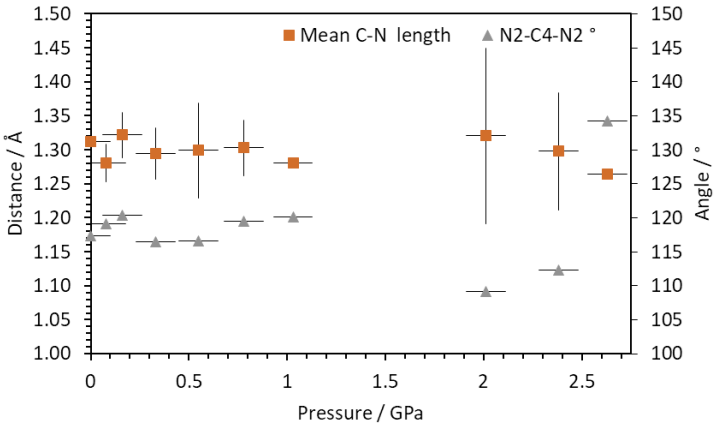

Figure S8: The change in the C-N bond lengths in the guanidinium cation and N2-C4-N2 angle shows the cation remaining rigid up to higher pressures.

Hirschfeld surfaces are a powerful tool for summarising and visualising intermolecular interactions. They are generated as an enclosed surface around a chosen molecule by assessing the promolecular electron density with the procrystal electron density using the Crystal Explorer software package.[14] The d_{norm} surfaces are coloured by mapping the internal distance of an atom (d_i) to the surface with an external contact atom (d_e) to the surface. The shorter distances are highlighted in red on the surface through white to blue as the contacts become longer. Plotting d_i vs d_e gives a 2D summary plot that fingerprints the inter-atomic contact environments of the molecule.[15]

The shorter the interatomic contact distance, the closer to the origin in the fingerprint plot. Intermolecular bonding interactions are usually sharp features which indicate directionality, whilst van der walls interactions and steric strain are usually more diffuse features (indirectional interactions).

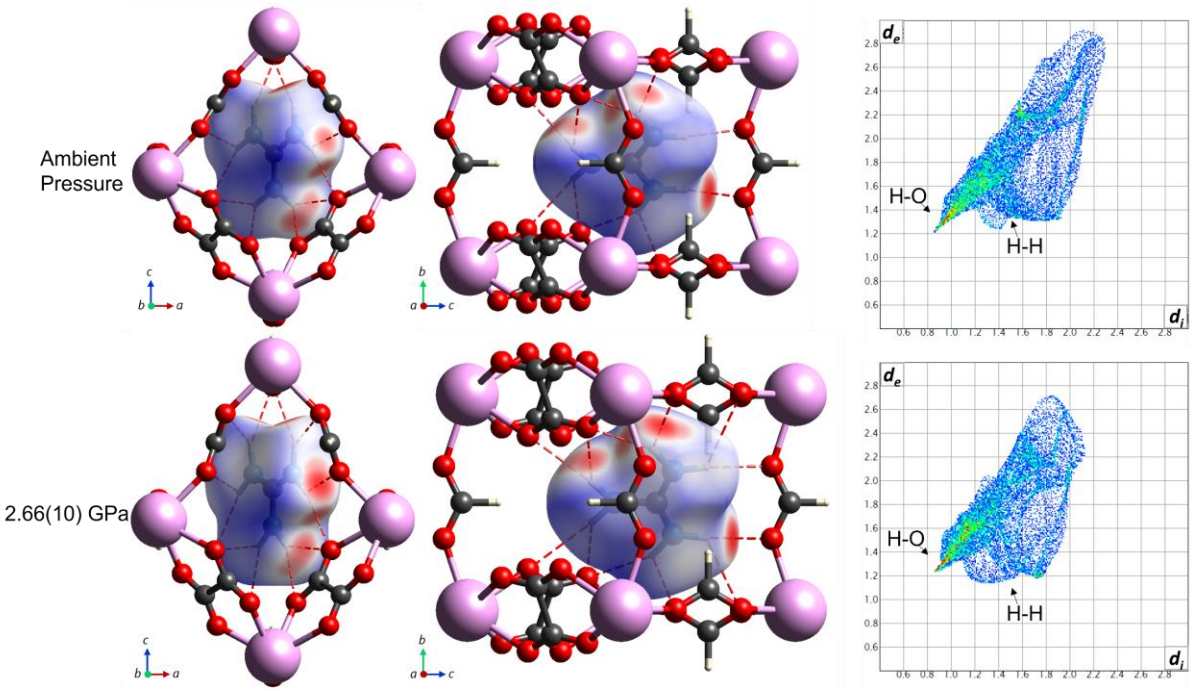

Figure S9: d_{norm} Hirschfeld surfaces generated around the guanidinium A-site cation in **GUA** at ambient pressure and at 2.66(10) GPa, just below the onset of crystal degradation. Summarised interactions are on respective fingerprint plots.

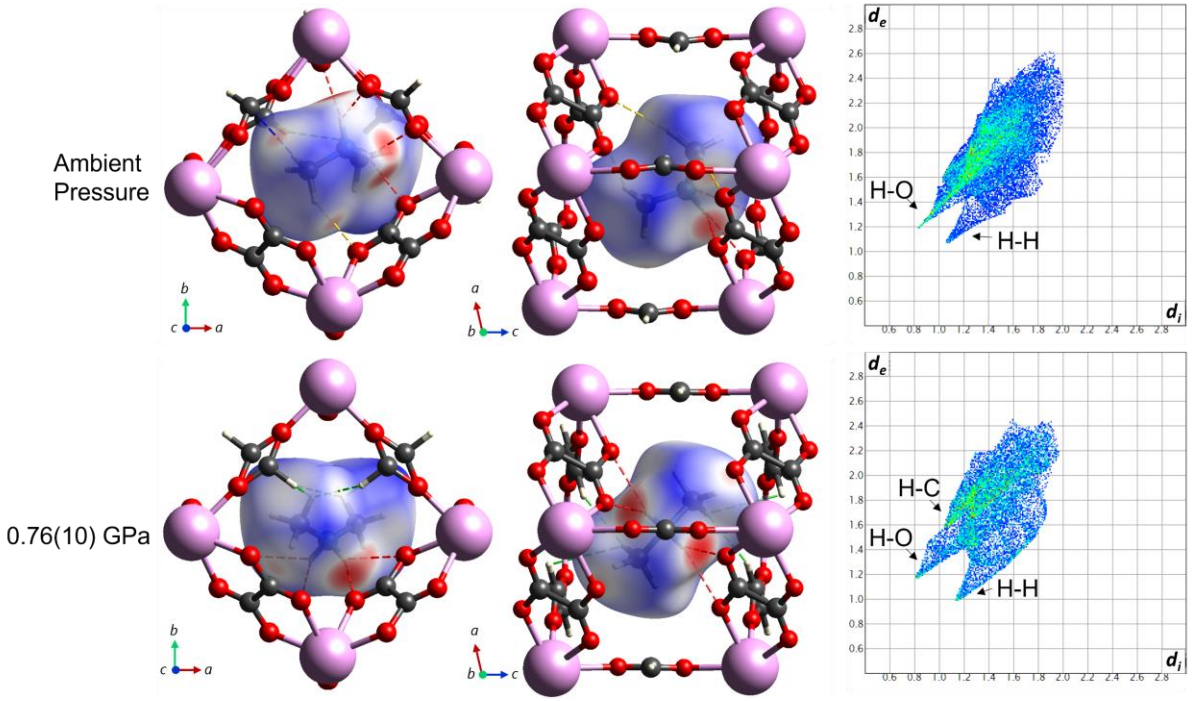

Figure S10: d_{norm} Hirschfeld surfaces generated around the DMA A-site cation in **DMA** at ambient pressure and at 0.76(10) GPa, just above the phase transition. Summarised interactions are on respective fingerprint plots.

The overall shift in the plots to lower d_e is representative of the compressing intermolecular interactions as the intramolecular interactions remain relatively rigid (Figure S8), usually observed under compression.[16] The exception to this is the sharp feature in the **GUA** plot which shows very subtle lengthening as the guanidinium cation retreats from one side of the cavity in favour of retaining the N2-H···O2 hydrogen bond and the anisotropic nature of the host-guest interactions, with some lengthening and others compressing.

The sharp features in the fingerprint plot for phase I of **DMA,** have a higher frequency of short O···H contacts indicated by the intensity (green), showing strong directional supramolecular interactions. In phase II the contact distances are shorter, but the features are broader, suggesting the intermolecular bonding is less directional, and some level of strain is occurring. This is also shown in the frequency of interaction types shifting to a more diffuse centre. This means that these intermolecular interactions, although shorter, may not be as strong as in phase I. A similar effect can be seen on the H-H contact types for all phases.

The percentage contributions to the Hirschfeld surface area filtered by interaction types represented in the fingerprint plots at ambient pressure are summarised by proportion in Figure S11, to highlight the differences in cation environment between the two systems.

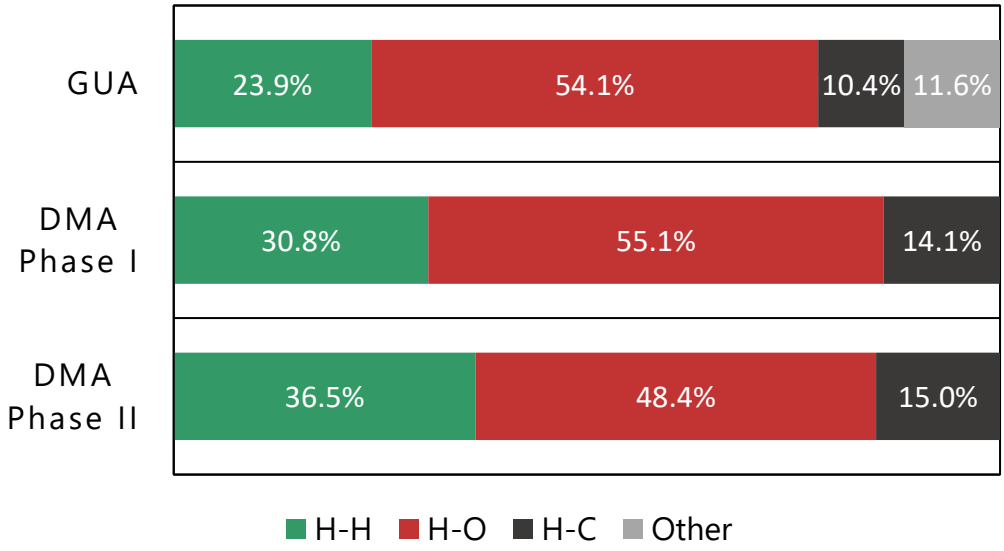

Figure S11: The host-guest contact environments (d_i – d_e) between **GUA** at ambient pressure phase I of **DMA** at ambient pressure and phase II. Other describes contacts of < 6 %, including H-N and N-C contacts that can form in **GUA** as a consequence of the planar geometry of the guanidinium cation.

There is no way to efficiently pack spherical objects in 3D space to a 100 % packing density; consequently, all crystals contain voids. A common approach to calculate the void space in a crystal is to define a probe of a given diameter and allow this to intercalate into the crystal structure to give a volume and surface area of the void dependent on the diameter of the probe and van der walls radii of the atoms. These are known as the solvent accessible voids, which are useful in cases where the adsorption capacity of sorbates is sought. This approach, however can underestimate the total void volume in a crystal due to leaving solvent inaccessible voids unaccounted for. Under hydrostatic pressure, all voids in a crystal will compress, including solvent inaccessible voids, so using the approach in Crystal Explorer where the void surface is calculated for the whole unit cell, with an isovalue of 0.002 eau^{-3}, the changes in total void space can be observed under increasing pressure.

Differences in linker rigidity are further confirmed by the changes in void space in **GUA**, Fig. S12, where voids are preferentially compressed around the formates whilst those around the oxalate are maintained at higher pressures.

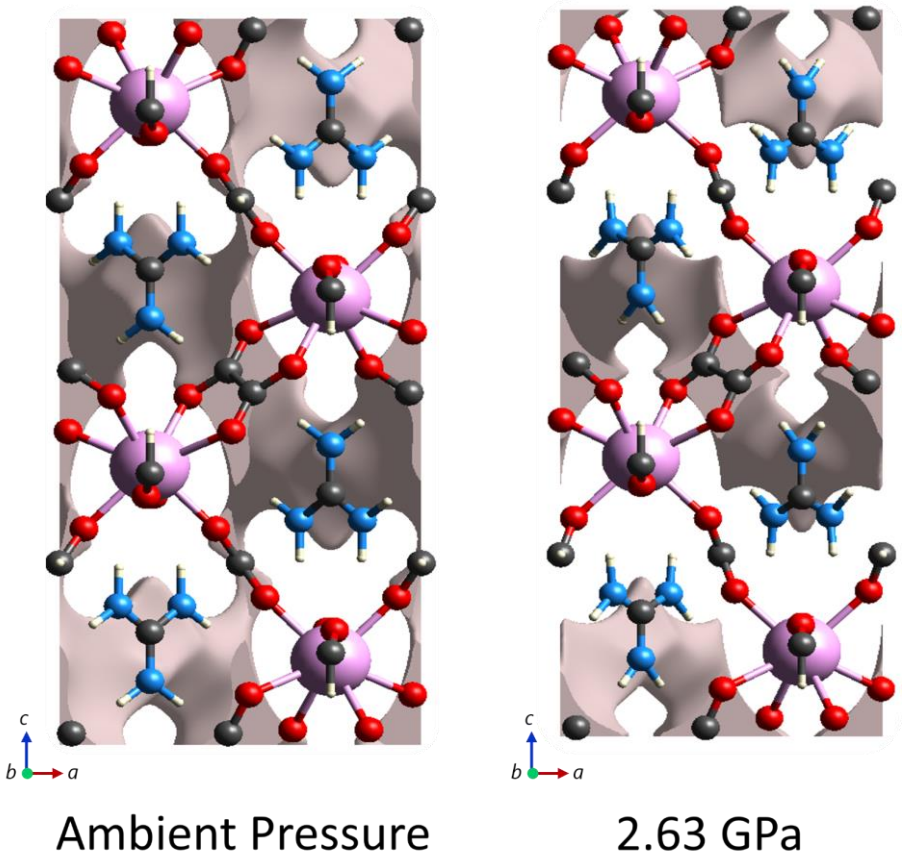

Figure S12: Void space calculated using crystal explorer for **GUA** at ambient pressure and 2.63 GPa showing regions of preferential compression.

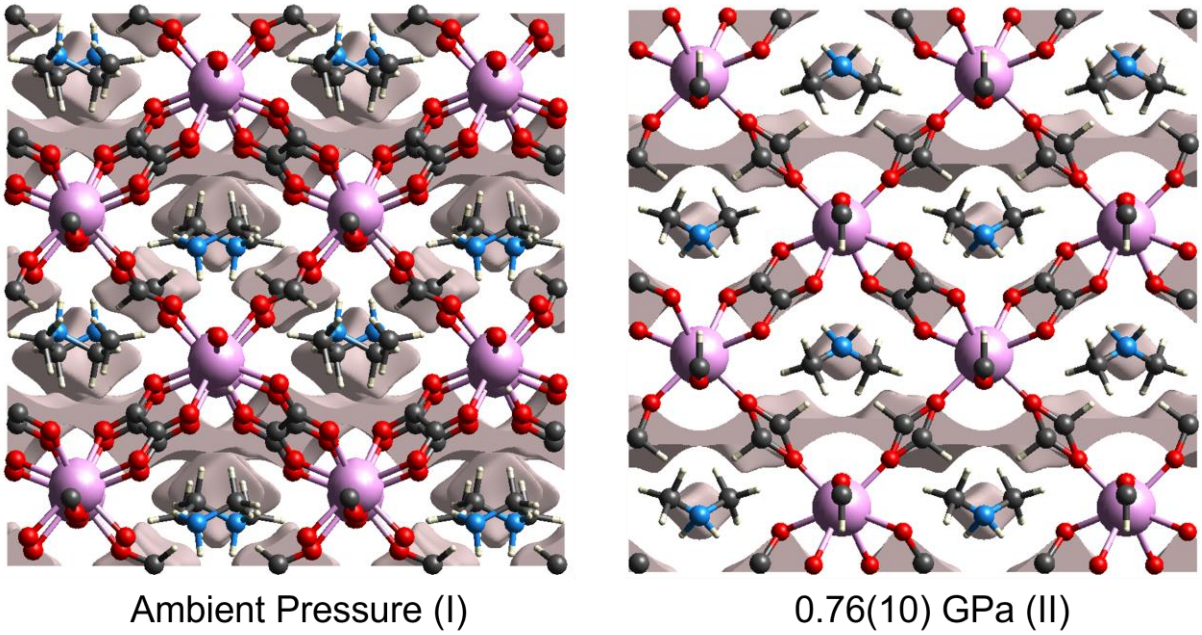

Figure S13: Void space calculated in crystal explorer for **DMA** with varying pressure showing relatively homogenous compression.

Table S12: Void surface properties for **GUA**.

Pressure/ GPa	Ambient	0.08	0.16	0.33	0.55	0.78	1.03	2.01	2.38	2.63
Void volume/ Å^3	118.18	117.19	112.40	107.52	102.63	100.98	96.71	75.55	71.60	71.20
Surface Area/ Å^2	331.47	324.00	315.23	307.92	302.13	293.30	285.64	237.25	237.48	231.26
Voids / %	10.99	10.96	10.58	10.21	9.80	7.55	7.18	7.21	9.68	9.35
Crystal Density / g cm^{-3}	2.503	2.518	2.534	2.556	2.571	2.691	2.699	2.725	2.582	2.602

Table S13: Void surface properties of **DMA**

Pressure/ GPa	Ambient	0.08	0.16	0.22	0.37	0.76	1.02	1.15	1.40
Void volume/ Å^3	89.14	86.84	81.90	85.51	77.91	34.49	32.84	35.18	26.55
Surface Area/ Å^2	278.99	278.74	265.49	275.33	258.23	113.31	114.24	110.89	96.18
Voids / %	8.27	8.05	7.67	7.99	7.33	6.55	6.27	6.79	5.22
Crystal Density / g cm^{-3}	2.412	2.411	2.436	2.429	2.447	2.470	2.483	2.508	2.554

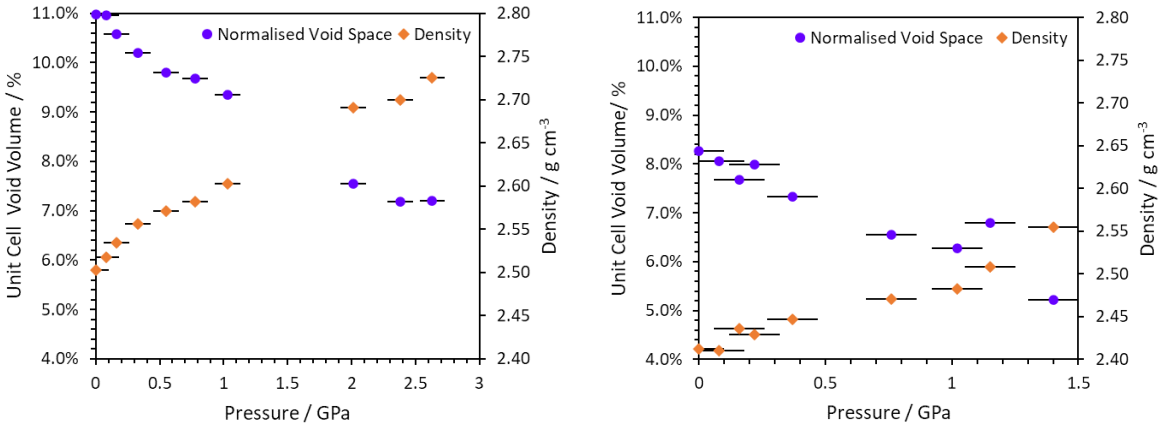

Figure S14: Void volume normalised against the volume of the unit cell showing the compression of the voids with increasing pressure and crystal density which increases with pressure for (left) **GUA** and (right) **DMA**.

For **GUA** the voids compress more sharply at lower pressures and could indicate a slight pressure dependence. The densification of **GUA** certainly shows this with the density initially increasing sharply. For **DMA** the compression of the voids and densification is at a consistent rate across the phase transition. The voids in **GUA** show preferential compression of the regions in the crystal around the formate linker with the voids around the oxalate linkers retained, showing a difference in linker rigidity. For **DMA** the voids compress around the oxalate in phase II, with more space around the formate disorder (although the disorder components positions are considered in tandem when generating the surface so the void volume may be artificially lower in these cases).

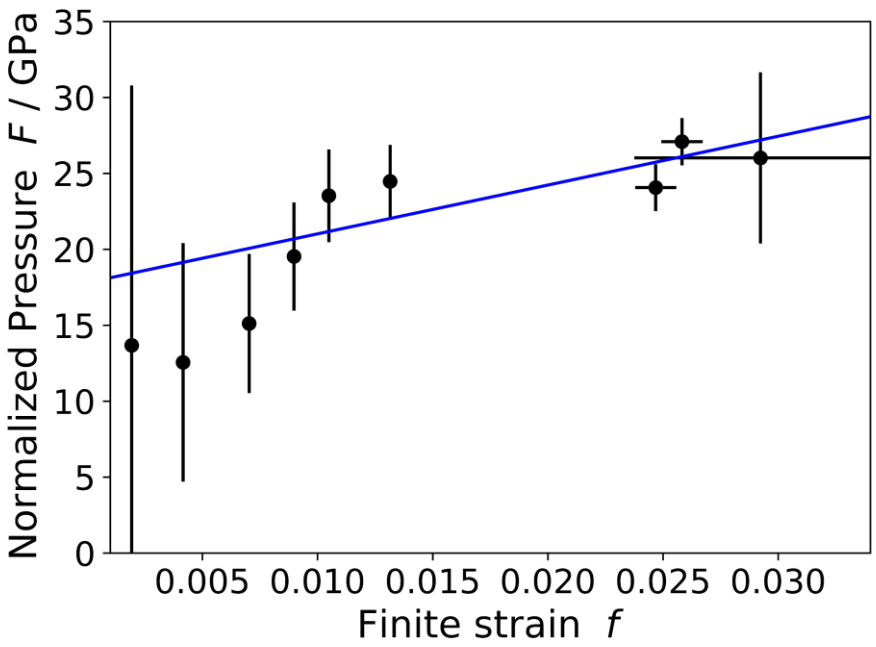

Figure S15: strain – normalised pressure (*F-f*) plot for **GUA** showing produced and fitted using EoS fit.[12,13]

References

1 L. G. Burley, J. H. Beecham-Lonsdale, A. K. Srivastava, I. E. Collings and P. J. Saines, *Dalt. Trans.*, 2021, **50**, 5437–5441.

2 T. R. R. McDonald and J. M. Spink, *Acta Crystallogr.*, 1967, **23**, 944–949.

3 H. Nowell, S. A. Barnett, K. E. Christensen, S. J. Teat and D. R. Allan, 2012, **19**, 435–441.

4 G. Winter, *J. Appl. Crystallogr.*, 2010, **43**, 186–190.

5 K. Diederichs, J. Beilsten-Edmands, G. Winter, R. Gildea, J. Parkhurst, D. Waterman and G. Evans, *Res. Pap. Acta Cryst*, 2020, **76**, 385–399.

6 G. Winter, D. G. Waterman, J. M. Parkhurst, A. S. Brewster, R. J. Gildea, M. Gerstel, L. Fuentes-Montero, M. Vollmar, T. Michels-Clark, I. D. Young, N. K. Sauter and G. Evans, *Res. Pap. Acta Cryst*, 2018, **74**, 85–97.

7 G. M. Sheldrick, *Acta Crystallogr. Sect. C Struct. Chem.*, 2015, **71**, 3–8.

8 O. V. Dolomanov, L. J. Bourhis, R. J. Gildea, J. A. K. Howard and H. Puschmann, *J. Appl. Crystallogr.*, 2009, **42**, 339–341.

9 C. J. McMonagle, G. F. Turner, I. Jones, D. R. Allan, M. R. Warren, K. V. Kamenev, S. Parsons, P. A. Wright and S. A. Moggach, *Chem. Commun.*, 2022, **58**, 11507–11510.

10 A. B. Cairns and A. L. Goodwin, *Phys. Chem. Chem. Phys.*, 2015, **17**, 20449–20465.

11 M. J. Cliffe and A. L. Goodwin, *J. Appl. Crystallogr.*, 2012, **45**, 1321–1329.

12 J. Gonzalez-Platas, M. Alvaro, F. Nestola and R. Angel, *urn:issn:1600-5767*, 2016, **49**, 1377–1382.

13 R. J. Angel, J. Gonzalez-Platas and M. Alvaro, *Zeitschrift fur Krist.*, 2014, **229**, 405–419.

14 P. R. Spackman, M. J. Turner, J. J. McKinnon, S. K. Wolff, D. J. Grimwood, D. Jayatilaka and M. A. Spackman, *J. Appl. Crystallogr.*, 2021, **54**, 1006–1011.

15 M. A. Spackman and J. J. McKinnon, *CrystEngComm*, 2002, **4**, 378–392.

16 P. A. Wood, J. J. McKinnon, S. Parsons, E. Pidcock and M. A. Spackman, *CrystEngComm*, 2008, **10**, 368–376.